Nanoscale

COMMUNICATION

View Article Online
View Journal | View Issue

Cite this: *Nanoscale*, 2022, **14**, 16427

Received 10th July 2022,
Accepted 11th October 2022

DOI: 10.1039/d2nr03770j

rsc.li/nanoscale

One-dimensional metal thiophosphate nanowires by cluster assembly†

Chanjuan Shang, Yanyan Zhao, Yan Su, Si Zhou * and Jijun Zhao

One-dimensional (1D) atomic wires with precise structures are not only excellent platforms for exploring novel 1D physics, but also promising building blocks to assemble functional materials and devices. However, stable atomic wires remain limited and are hard to search using global optimization algorithms. Inspired by the emerging layered ternary chalcogenides, here we offer a design strategy for rational assembly of metal thiophosphate (MPS_4) nanowires based on the concept of a superatom. *ortho*-Thiophosphate [PS_4] clusters are linked by proper main-group and transition metal atoms to form closed electronic shells, endowing the assembled nanowires with high dynamic and thermal stabilities. Diverse and exotic electronic band structures are hosted by these ternary MPS_4 nanowires, such as the coexistence of a spin–orbit Dirac point protected by nonsymmorphic symmetry and a flat band near the Fermi level, with nanowires being bipolar magnetic semiconductors for electrical control of spin orientation. These 1D Lego blocks can be further built into higher-order architectures *via* vdW interaction or covalent bonding. This assembly approach generally produces stable atomic wires with designated compositions and structure symmetries to induce peculiar quantum states for future applications.

Key Laboratory of Materials Modification by Laser, Ion and Electron Beams (Dalian University of Technology), Ministry of Education, Dalian 116024, China.
E-mail: sizhou@dlut.edu.cn

† Electronic supplementary information (ESI) available: Detailed structural parameters, stability, and electronic properties results of 1D, 2D and bulk MPS_4. See DOI: https://doi.org/10.1039/d2nr03770j

Si Zhou

Dr Si Zhou is a professor at the School of Physics at Dalian University of Technology. She has focused on cluster science and low-dimensional materials using theoretical methods such as first-principles calculations and genetic algorithms. Her achievements include the prediction of many innovative low-dimensional structures for electronics, spintronics, optics, and energy conversion, some of which have been realized in experiments. She has published over 90 peer-reviewed articles as the first- or corresponding-author in Chem. Rev., J. Am. Chem. Soc., Angew. Chem., Int. Ed., Nano Lett., ACS Nano, etc., *with citations numbering over 6000 and an H-index of 39.*

Introduction

With the boom of two-dimensional (2D) layered materials, searching for atomic-scale Lego blocks has aroused tremendous interest. Artificial nanostructures with peculiar physical properties and integrated devices with multiple functions can be conveniently constructed by assembly of these van der Waals (vdW) Lego units.[1] Stimulated by 2D transition metal dichalcogenides (TMDs) and trihalides, 1D atomic wires of binary transition metal compounds with various stoichiometries have been synthesized in experiments, such as the isolated chains of M_6X_6 (M = Mo, W; X = S, Se, Te)[2–5] and Mo_5S_4,[6] and the single-chain or the few-chain MTe_3 (M = Ti, Hf, Nb, V)[7,8] and NiY_2 (Y = Cl, Br)[9] stabilized in carbon nanotubes. The geometrical structures and fundamental properties of binary nanowires with different stoichiometries have been theoretically explored and compared with their 2D counterparts.[10–13] Intriguingly, most 1D transition metal chalcogenide nanowires exhibit metallic behavior, while a large number of TMD monolayers are semiconductors.[14–16] Transition metal halide nanowires present diverse electronic and magnetic properties, somewhat similar to reported 2D halides (*e.g.* CrI_3, $FeCl_2$, and VI_3) that comprise magnetic semiconductors and half metals.[17–20]

Recently, ternary metal phosphorus trichalcogenides in the form of MPX_3 (M = Mn, Fe, Co, Ni, Cu, Zn, Cd, *etc.*; X = S, Se)

emerged as a new family of 2D materials.[21] They have a common layered structure with $(P_2X_6)^{4-}$ bipyramids arranged in a triangular lattice that sandwich the metal layer. The MPX_3 monolayers have moderate band gaps of 1.5–3.5 eV falling in the range of visible light wavelengths, and are thereby attractive for optoelectronics, photodetectors, and photocatalysts.[22] Intrinsic long-range magnetic order exists in some 2D ternary compounds. For instance, antiferromagnetism is observed in $MnPS_3$, $FePS_3$, and $NiPS_3$ monolayers.[23] $MnPS_3$ exhibits the anisotropic behavior of magnetic moments, capable of coupling the valley degree of freedom to the antiferromagnetic order.[24] The $CuInP_2S_6$ crystal and thin films have been demonstrated to be ferroelectric with an order to disorder transition temperature of 315 K. An out-of-plane electric polarization has been predicted for the $CuInP_2S_6$ monolayer.[25]

Apparently, greater chemical diversity and structural complexity would induce richer physics in the 2D ternary compounds with regard to 2D binary chalcogenides and halides. It brings intriguing questions as to whether the atomic wires of ternary transition metal compounds can stably exist. How do their electronic structures depend on the elemental composition? How do their fundamental properties compare with those of their 2D counterparts? Computational screening the existing bulk materials with layered or chain-like structures has led to the discovery of many 2D and 1D materials.[26–28] The theoretical exfoliation energies can be used to evaluate the possibility for cleaving low-dimensional building blocks from their bulk crystals, that is, growth by the "top-down" approach. Then, the elemental substitution is useful to further extend the chemical compositions of monolayers or chains. However, such conventions only predict 2D and 1D materials with very limited structures, and omit a large number of possible structures that may be fabricated by the "bottom-up" approach on proper substrates or templates.

Here we develop a strategy for the rational design of 1D metal thiophosphate nanowires in the form of MPS_4 by cluster assembly. Based on the concept of a superatom, *ortho*-thiophosphate $[PS_4]$ units are linked by selective main-group metal atoms and transition metal atoms, such that the tetrahedral $[PS_4]$ cluster has a magic number of electrons to satisfy the electronic-shell closure. Following this assembly rule, a total of 26 MPS_4 nanowires are constructed. Their energetic, dynamic, and thermal stabilities are comprehensively examined by density functional theory (DFT) calculations to validate our assembly rule. The electronic and magnetic structures of these MPS_4 nanowires are investigated to illuminate their potential for device applications. The stable 1D MPS_4 building blocks are further exploited to assemble higher-order architectures.

Computational methods

DFT calculations were carried out by the Vienna *ab initio* simulation package (VASP),[29,30] using the planewave basis set with an energy cutoff of 500 eV, the projector augmented wave (PAW) potentials,[31,32] and the generalized gradient approximation (GGA)[33] parametrized by Perdew, Burke and Ernzerhof (PBE) for the exchange–correlation functional.[34] A vacuum space of 15 Å was applied to the directions perpendicular to the axial direction of MPS_4 nanowires. Uniform *k*-point meshes, with density 0.05 $Å^{-1}$ and 0.0002 $Å^{-1}$, were used to sample the Brillouin zone of the nanowires for geometry optimization and band structure calculation, respectively.[35] The cell parameters of MPS_4 nanowires along the axial direction were fully optimized and the ionic positions were relaxed with the convergence criteria for total energy and force of 10^{-5} eV and 0.01 eV $Å^{-1}$, respectively. The Heyd–Scuseria–Ernzerhof (HSE06) hybrid functional[36] was used to calculate the electronic band structures of simple metal thiophosphate nanowires assembled from group-IIIA atoms (B, Al, Ga, In) and $[PS_4]$ units, which predicts band gaps of about 1.2 eV larger than the values given by the PBE functional. For transition metal thiophosphate nanowires and monolayers, the DFT+*U* method[37] was adopted to compute their band structures to account for the strong correlation effect. For consistency, we used the Hubbard on-site Coulomb parameter $U = 3$ eV for all the transition metal MPS_4 nanowires. The obtained electronic band structures have features similar to those calculated by the PBE functional. Other *U* values were also tested, which generally affect the band gap, but do not influence the metallic systems. The detailed results obtained *via* different methods are compared in Table S1 and Fig. S1 of the ESI.† The phonon dispersion was calculated by the Phonopy code[38] interfaced with the density functional perturbation theory (DFPT) implemented in VASP. The thermal stability of the assembled MPS_4 nanowires was characterized by *ab initio* molecular dynamics (AIMD) simulations implemented in VASP. The molecular orbitals of a $[PS_4]^{3-}$ cluster and natural population of the on-site charge were calculated by the Gaussian16 package,[39] using the PBE functional accompanied with LANL2DZ basis sets.

Results and discussion

To design metal thiophosphate nanowires, we consider the *ortho*-thiophosphate $[PS_4]$ units in a tetrahedral geometry linked by metal atoms to form a chain, as illustrated in Fig. 1a. The rule for assembling MPS_4 nanowires is to reach stable electronic configurations for both $[PS_4]$ clusters and M atoms after their bonding. For highly symmetric clusters, the jellium model suggests that the molecular orbitals generated by valence electrons resemble the shapes of atomic orbitals.[40] A cluster will have enhanced stability when its number of valence electrons coincides with a closed-shell structure (so-called "magic number"). For a tetrahedral cluster with T_d symmetry, the molecular orbitals split in energy and the magic numbers can be determined as 2, 8, 10, 16, 20, 26, 32, *etc*.[41] As a free $[PS_4]$ unit carries 29 valence electrons, it has to gain three electrons from the M linkers to reach a magic number and electronic-shell closure. Intuitively, group-IIIA atoms (B, Al, Ga, and In) with three valence electrons, as well as tran-

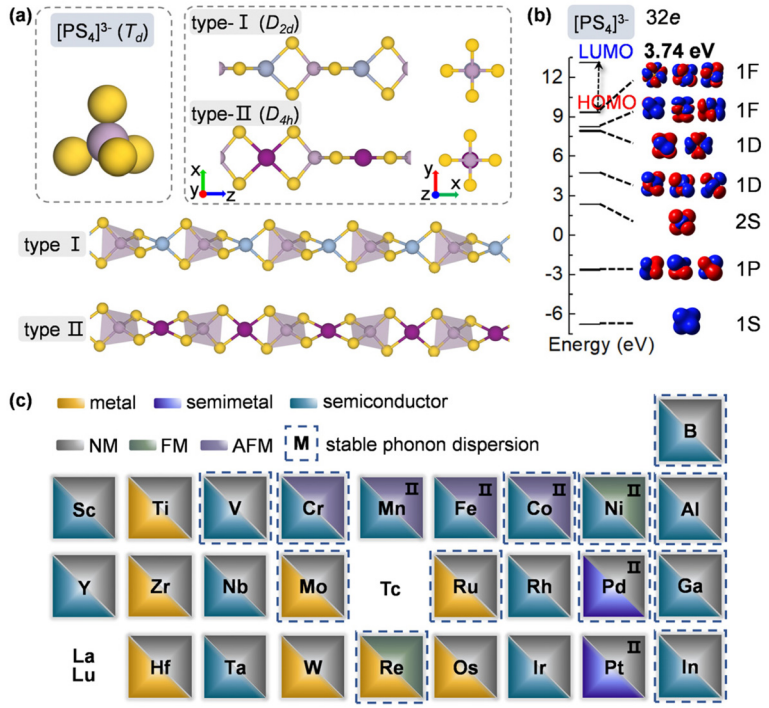

Fig. 1 (a) Geometrical structure of a $[PS_4]^{3-}$ cluster (top left panel) and the assembled 1D MPS_4 nanowire (top right panel and bottom two panels) from different views. The P, S, and M atoms are shown in purple, yellow, and blue (magenta) colors, respectively. (b) Energy diagrams and molecular orbitals of $[PS_4]^{3-}$. The energy is relative to the vacuum level. The HOMO–LUMO gap is given. (c) Electronic and magnetic properties of 1D MPS_4 nanowires, where M is either a transition metal element or a group-IIIA element. The dashed boxes indicate nanowires with a stable phonon dispersion. The systems with type-II structures are indicated by the symbol "II" in the upper right corner.

sition metal elements with open d shells and exhibiting variable oxidation states, may satisfy such criteria and form stable 1D nanowires with the $[PS_4]$ unit.

Next, we constructed MPS_4 nanowires by linking $[PS_4]$ clusters with group-IIIA and transition metal atoms. To determine the ground-state geometry and magnetic order, we adopted different supercells ($1 \times 1 \times 2$ and $1 \times 1 \times 4$ unit cells) to arrange the adjacent $[PS_4]$ clusters in different orientations and tested different spin configurations for the magnetic atoms. As displayed in Fig. 1a, the two most stable structure phases are found for the assembled MPS_4 nanowires. In the type-I configuration, the adjacent $[PS_4]$ clusters are in the same orientation, such that each M atom stays in the center of S_4 tetrahedra as that of a P atom. The nanowire has D_{2d} symmetry and an M–S–P angle of about 90°. In the type-II configuration, the two adjacent $[PS_4]$ units rotate by 90° along the axial direction, such that each M atom stays in the center of the S_4 rectangle, resulting in D_{4h} symmetry for the nanowire.

Upon geometry optimization, all the considered 1D chains are stable. For both phases, the $[PS_4]$ unit in the nanowire well maintains its tetrahedral structure. We examined the molecular orbitals of a free $[PS_4]^{3-}$ ion, which mimics the $[PS_4]$ building block in the MPS_4 nanowires. It exhibits highly symmetric superatomic orbitals, as displayed in Fig. 1b. The 32 valence electrons fill the electronic shell of $1S^21P^62S^21D^{10}1F^61F^6||1F^0$ under the symmetry-adapted orbital model,[41,42] where the 1F orbital splits and the two lower energy levels are fully occupied, with a large gap of 3.74 eV between the highest occupied molecular orbital (HOMO) and lowest unoccupied molecular orbital (LUMO). These results manifest the superatomic nature of the tetrahedral $[PS_4]$ cluster and indicate its high stability by gaining a proper number of electrons when assembled into MPS_4 nanowires.

The ground-state structure phases, electronic and magnetic properties, and dynamical stabilities of the assembled MPS_4 nanowires are summarized in Fig. 1c. Most of these 1D systems prefer the type-I structure with D_{2d} symmetry, while six MPS_4 nanowires (M = Mn, Fe, Co, Ni, Pd, and Pt) have the type-II structure with D_{4h} symmetry. In particular, there are 12 MPS_4 nanowires that have stable phonon dispersions (Fig. 2a and Fig. S2†), comprising either the group-IIIA elements (M = B, Al, Ga, and In) or selective transition metal elements (M = V, Cr, Co, Ni, Mo, Re, Ru, and Pd). We have also tested some other main group elements, such as those elements from group-IA (Na), group-IIA (Mg), group-IVA (Sn, Pb), and group-VA (Bi). Their assembled 1D MPS_4 structures are either broken down during optimization or have unstable phonon dispersions, which in turn corroborate our proposed assembly criteria. In the following content, we will focus on the 12 MPS_4 nanowires that are dynamically stable.

The thermal stability of MPS_4 nanowires was assessed by an AIMD simulation. As depicted in Fig. 2b and Fig. S3,† single

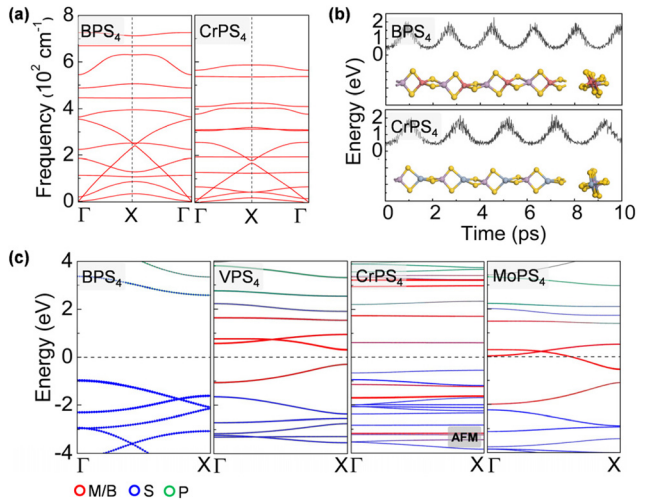

Fig. 2 (a) Phonon dispersions of BPS_4 and $CrPS_4$ nanowires. (b) Energy profile during AIMD simulation for BPS_4 and $CrPS_4$ nanowires at 300 K. The energy is referred to that of the equilibrium structure at 0 K. The insets are snapshot structures at 10 ps (left: side-view; right: top-view). The M, P, and S atoms are shown in blue (pink), purple, and yellow colors, respectively. (c) Electronic band structures of selective MPS_4 nanowires. The contributions from different atoms are shown by color. The Fermi level is shifted to zero (dashed lines).

chains of MPS_4 have outstanding thermal stability at 300 K. The structure does not show any noticeable distortion during a simulation time of 10 ps. Taking the BPS_4 and $CrPS_4$ nanowires as representatives, the variations of M–S and P–S bond lengths are within 0.14 Å and 0.19 Å for BPS_4 and 0.16 Å and 0.12 Å for $CrPS_4$, respectively, signifying the structural robustness of these 1D ternary compound materials. We further characterized the energetic stability of 1D MPS_4 nanowires by their formation energy defined as,

$$E_{\text{form}} = E(\text{MPS}_4) - [E(\text{H}_3\text{PS}_4) - 3/2E(\text{H}_2)] - E(\text{M}) \quad (1)$$

where $E(MPS_4)$, $E(H_3PS_4)$, and $E(H_2)$ are the total energies of MPS_4 nanowire per formula, a free H_3PS_4 and H_2 molecule, respectively; $E(M)$ is the energy of the M atom in its most stable bulk form. As presented in Tables 1 and 2, group-IIIA MPS_4 (M = B, Al, Ga, In) and 3d transition metal MPS_4 (M = V, Cr, Co Ni) nanowires have negative values of E_{form} = −1.44 to −0.08 eV, while $MoPS_4$, $RuPS_4$, $PdPS_4$, and $RePS_4$ nanowires have positive E_{form} values. A negative value of E_{form} indicates that the formation of an MPS_4 nanowire by metal ion substitution of H_3PS_4 acid is exothermic. These proposed 1D MPS_4 nanowires may be synthesized by the assembly of $[PS_4]^{3-}$ ions, and group-IIIA metal atoms or transition metal atoms in 1D templates with a hollow cavity. A variety of transition metal chalcogenide and halide chains have been grown by vapor transport in open-ended carbon nanotubes and boron nitride nanotubes in the experiment.[3,43,44]

Table 1 Formation energy (E_{form}) and band gap (E_g) of 1D group-IIIA MPS_4 nanowires; inter-chain distance (d) and band gap (E_g) of the assembled 3D MPS_4

	1D		Bulk	
	E_{form} (eV)	E_g (eV)	d (Å)	E_g (eV)
BPS_4	−0.93	3.57	3.72	3.21
$AlPS_4$	−2.42	4.14	3.71	3.55
$GaPS_4$	−1.34	4.01	3.74	3.17
$InPS_4$	−0.80	3.73	3.82	3.12

Table 2 Magnetic state, band gap (E_g), magnetic moment (M), and exchange energy (E_m), of 1D transition metal MPS_4 nanowires and the assembled MPS_4 monolayers. Formation energy (E_{form}) is also given for 1D MPS_4. For ferromagnets, band gaps for spin-up and spin-down channels are provided

1D	State	E_g (eV)	M (μ_B)	E_m (meV)	E_{form} (eV)
VPS_4	NM	0.60	—	—	−1.21
$CrPS_4$	AFM	1.15	2.78	−99	−1.44
$CoPS_4$	AFM	0.81	1.53	−8	−0.16
$NiPS_4$	FM	1.73/0.22	0.51	26	−0.08
$MoPS_4$	NM	Metal	—	—	0.13
$RuPS_4$	NM	Metal	—	—	0.69
$PdPS_4$	NM	0	—	—	0.06
$RePS_4$	FM	1.41/metal	0.92	44	1.06

2D	State	E_g (eV)	M (μ_B)	E_m (meV)
VPS_4	AFM	0.03	1.80	−15
$CrPS_4$	FM	0.66/1.69	2.91	6
$CoPS_4$	NM	0.71	—	—
$NiPS_4$	AFM	Metal	0.41	−27
$MoPS_4$	NM	Metal	—	—
$RuPS_4$	NM	0.37	—	—
$PdPS_4$	NM	Metal	—	—
$RePS_4$	NM	Metal	—	—

The electronic band structures of the assembled MPS_4 nanowires are given in Fig. 2c, 3, 4 and Fig. S4.† The group-IIIA MPS_4 (M = B, Al, Ga, and In) nanowires are semiconductors with large band gaps of 3.57–4.14 eV predicted by the HSE06 hybrid functional. Encouragingly, these 1D ternary compounds exhibit diverse electronic and magnetic properties, including those of semiconductors, metals, semimetals, and ferromagnetic and antiferromagnetic semiconductors, and thereby serve as a rich family of 1D candidates for electronics, spintronics, and optoelectronics. We calculated the magnetic anisotropy energy (MAE) given by the energy difference of the magnetization direction parallel and perpendicular to the axial direction. Most of the magnetic MPS_4 nanowires have the easy-axis perpendicular to the chain with MAE values of 0.02–0.75 meV per magnetic atom. Only the $CoPS_4$ nanowire has the spin orientation along the chain direction in an antiferromagnetic order. As shown by the electronic band structures in Fig. 2c and Fig. S4,† $CrPS_4$ and $CoPS_4$ nanowires are both antiferromagnetic semiconductors with band gaps of 1.15 and 0.81 eV and magnetic moments of 2.78 and 1.53μ_B per metal atom, respectively. The VPS_4 nanowire is a non-magnetic semiconductor with band gap of 0.60 eV, while the single chains of $MoPS_4$ and $RuPS_4$ exhibit metallic behavior. It is worth mentioning that

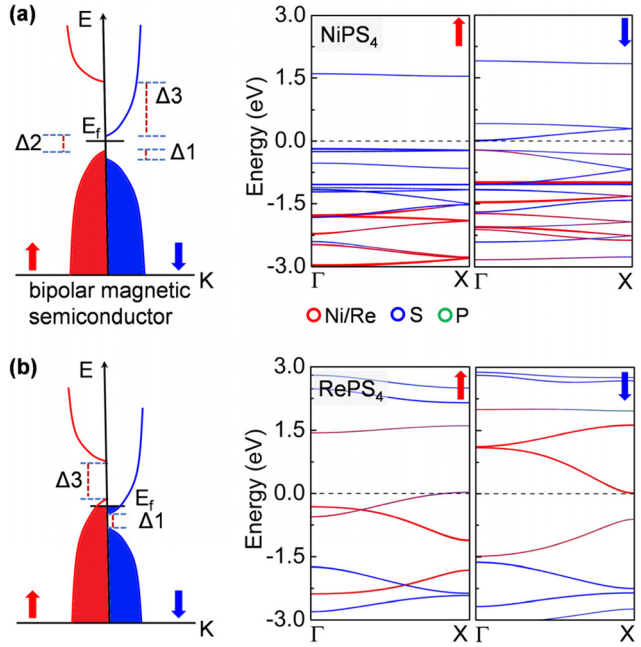

Fig. 3 Electronic band structures of (a) $NiPS_4$ and (b) $RePS_4$ nanowires. The contributions from different atoms or orbitals are shown by the colors. The Fermi level is shifted to zero (red dashed lines). The left panels are schematic plots of their band structures.

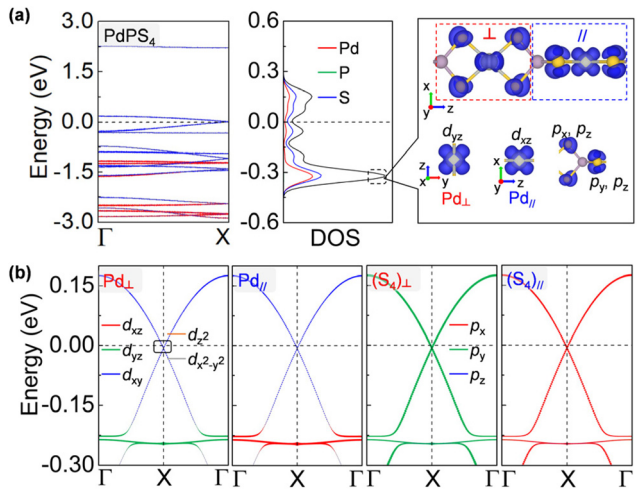

Fig. 4 (a) Electronic band structures and density of states (DOS) of a $PdPS_4$ nanowire calculated without SOC. The right panel displays the partial charge density of the flat band at about −0.3 eV. (b) Band structure of a $PdPS_4$ nanowire calculated with SOC. The contributions from different atoms or orbitals are shown by the colors. The Fermi level is shifted to zero (dashed lines).

the $CoPS_4$ nanowire can have a non-collinear magnetic order, with the preference of spin orientation alternately parallel and perpendicular to the wire, as shown in Fig. S5.† However, the energy of the non-collinear magnetic order is 1.6–4.8 meV per Co atom higher than that of the collinear antiferromagnetic ground state.

Remarkably, the $NiPS_4$ nanowire is a bipolar magnetic semiconductor, as is featured by its different conduction band minimum (CBM) and valence band maximum (VBM) in terms of electronic spins.[45] As shown in Fig. 3a, the VBM and CBM are contributed to by the majority and minority spin carriers, respectively, both from S atoms. There is a small gap of 0.20 eV, termed the spin–flip gap (Δ_2), between VBM and CBM. By applying a small positive (negative) gate voltage, the minority (majority) spin carriers are created, allowing for the electrical control of these carriers' spin orientations. The spin splitting near the Fermi level is mainly contributed to by S atoms. The $RePS_4$ chain exhibits similar features to that of $NiPS_4$, but has no gap at the Fermi level. As displayed in Fig. 3b, the spin-up and spin-down channels are slightly doped. The electronic states near the Fermi level are dominated by Re atoms. When applying a small gate voltage, minority spin carriers are generated with a large spin-conserved gap (Δ_3) of 1.46 eV, while a negative gate voltage is required to generate majority spin carriers with a large spin-conserved gap (Δ_1) of 0.62 eV. Therefore, these nanowires can carry completely spin-polarized currents under a proper electric field, allowing for exciting applications, such as a bipolar field effect spin filter and field effect spin valve, as well as detection and separation of entangled electrons from superconductors for quantum information processing.[46]

More impressively, the $PdPS_4$ nanowire in the type-II configuration is a semimetal that is robust against spin–orbit coupling (SOC) protected by its nonsymmorphic symmetry.[47] As shown in Fig. 4a, the CBM and VBM touch each other nearly at the Fermi level. A gap is not opened by adopting denser k-points with 0.0001 $Å^{-1}$, larger SOC strength, or other U values (see Fig. S6†).[48] This type of Dirac point that is robust against SOC is termed a spin–orbit Dirac point (SDP) and is distinct in nature from the SOC-vulnerable Dirac point. It has been reported in some 2D materials, such as RhB_4,[49] MXenes[50] and $HfGe_{0.92}Te$.[51] Even more excitingly, the $PdPS_4$ chain simultaneously harbors SDP and a nearly flat band near the Fermi level (at about −0.2 eV). A flat momentum-energy dispersion is the singularity in density of states, and the charge carriers in it have a zero group velocity and an infinite effective mass. It has been realized in Kagome lattice systems, twisted bilayer graphene and transition metal diachalcogenides,[52–55] and may lead to high-temperature superconductivity, fractional Chern insulators, Wigner crystal formations, and so on.[56] According to the density of states in Fig. 4a and b, the flat band of a $PdPS_4$ nanowire is localized on the Pd–S_4 planar unit, contributed to by the S p orbital and Pd d orbital perpendicular to the Pd–S_4 plane. As the neighboring Pd–S_4 units are perpendicular to each other, their orbital hybridization is very weak, which may be the origin of the flat dispersion. Therefore, the $PdPS_4$ nanowire with its unique structure is a great 1D platform for exploring the coexistence of multiple exotic quantum states.

Next, we explore the possibility of assembling these 1D MPS_4 building blocks into higher-order architectures. The interaction between two MPS_4 nanowires is examined. Our

results show that the group-IIIA MPS_4 (M = B, Al, Ga, In) nanowires favor vdW interactions between neighboring chains, while the transition metal MPS_4 nanowires are covalently bonded when approaching each other. As a result, group-IIIA MPS_4 (M = B, Al, Ga, In) nanowires form quasi-1D bulk structures as illustrated in Fig. 5a. The supercell consists of parallel MPS_4 chains arranged in a rectangular lattice. The chains in the center and at the corner of the supercell are shifted along the axial direction. The vertical distance between the center atoms of two neighboring nanowires is about 6.0 Å, and the separation between the outermost S atoms of two neighboring nanowires is more than 3.7 Å (see Table 1), manifesting the vdW interactions between them. Accordingly, needle-shaped crystallites of the above quasi-1D BPS_4 and $AlPS_4$ have been synthesized experimentally.[57,58] Fig. 5c and Fig. S7† display the electronic band structures of three-dimensional (3D) MPS_4 by HSE06 calculations. The band gaps of bulk MPS_4 (M = B, Al, Ga, In) are reduced to 3.12–3.55 eV with regard to the single chains. The band along the inter-chain direction is dispersive owing to the moderate interaction between neighboring chains. The band dispersions along the inter-chain direction and axial direction are noticeably different, implying the anisotropic electronic transport behavior of these unique quasi-1D structures, which are desirable for certain device applications, such as anisotropic field effect transistors and photodetectors, thermoelectronics, and piezoelectric and ferroelectric devices.[59,60]

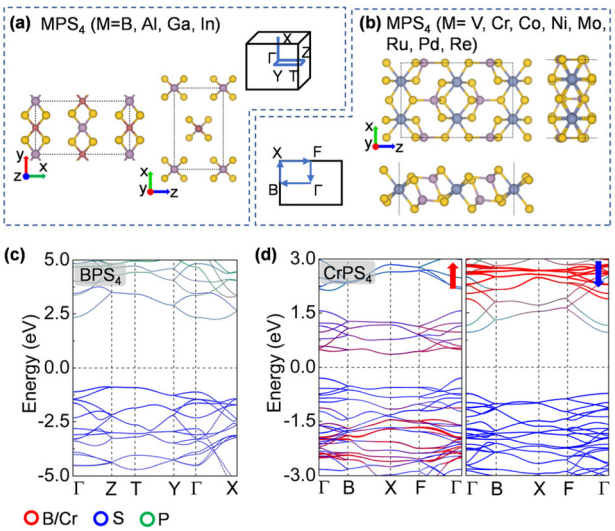

Fig. 5 (a) and (b) Atomic structures of assembled bulk MPS_4 (M = B, Al, Ga, In) and an MPS_4 (M = V, Cr, Co, Ni, Mo, Ru, Pd, and Re) monolayer, respectively, displayed from different perspectives. The M, P, and S atoms are shown in blue (pink), purple, and yellow colors, respectively. The corresponding Brillouin zones are illustrated. (c) and (d) Electronic band structures of assembled bulk BPS_4 and monolayer $CrPS_4$, respectively. The contributions from different atoms or orbitals are shown by color. The Fermi level is shifted to zero (dashed lines).

The transition-metal-containing MPS_4 (M = V, Cr, Co, Ni, Mo, Ru, Pd, and Re) nanowires favor covalent bonding between adjacent chains, leading to the formation of the monolayer structure shown in Fig. 5b. The tetrahedral [PS_4] unit is slightly deformed, while each Cr atom is six-fold coordinated by S atoms and surrounded by four [PS_4] units, resulting in an anisotropic rectangular lattice structure. Actually, such a layered structure of $CrPS_4$ has been synthesized in the experiment,[61,62] which again corroborates our proposed assembly rule for building stable nanostructures *via* [PS_4] clusters. As shown in Fig. 5d, the $CrPS_4$ monolayer is a ferromagnetic semiconductor with a magnetic moment of 2.91μ_B per Cr atom, and band gap of 0.66 eV and 1.69 eV for the spin-up and spin-down channels, respectively, in good agreement with previous theoretical reports.[63] The VPS_4 and $NiPS_4$ monolayers are antiferromagnets, while the others are non-magnetic (see Table 2 and Fig. S8† for details). The magnetic moment prefers to align perpendicular to the layer for all these 2D magnets.

The robustness of the magnetism in cluster-assembled 1D and 2D MPS_4 structures is evaluated by the exchange energy E_m, defined as the energy difference between the lowest-lying

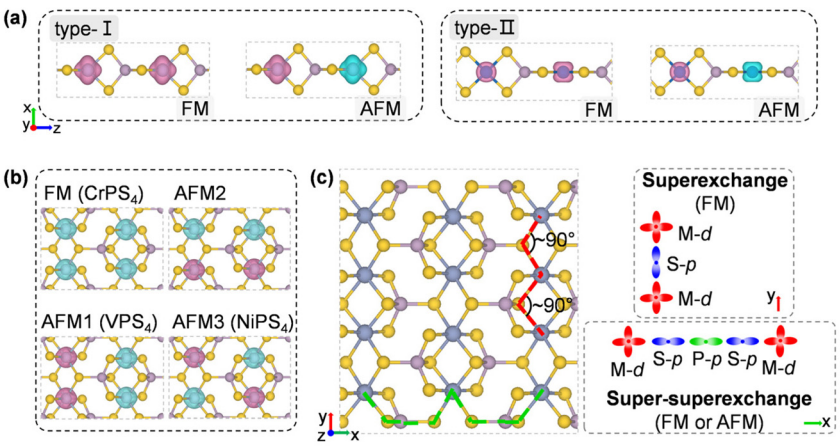

Fig. 6 (a) and (b) Spin density distributions of an MPS_4 nanowire and MPS_4 monolayer in FM and low-energy AFM states. The ground-state magnetic configuration is indicated for VPS_4, $CrPS_4$, and $NiPS_4$ monolayers, respectively. (c) Schematic illustration of superexchange and super-superexchange interactions for the MPS_4 monolayer.

antiferromagnetic state (E_{AFM}) and ferromagnetic state (E_{FM}) per MPS_4 formula *via*:

$$E_m = E_{AFM} - E_{FM} \quad (2)$$

Spin-polarized charge density distributions for FM and low-energy AFM configurations of 1D and 2D MPS_4 structures are presented in Fig. 6a and b. The 1D nanowires of $CrPS_4$, $CoPS_4$, $NiPS_4$ and $RePS_4$ have E_m = −99 meV, −8 meV, 26 meV, and 44 meV per formula unit (f.u.), respectively (Table 2). Their magnetic orders can be understood by the super-superexchange interaction along the M–S–P–S–M long superexchange interaction through the Cr–S–Cr bonds with a bond angle of about 90°, as shown in Fig. 6c.[64–67] VPS_4 and $NiPS_4$ monolayers are antiferromagnetic with E_m = −15 meV f.u.$^{-1}$ and −27 meV f.u.$^{-1}$, respectively. The former shows competition between FM and AFM coupling along the two in-plane directions, while the latter favors AFM order along both in-plane directions. As a reference, an existing 2D magnetic material like the CrI_3 monolayer has E_m = 28 meV f.u.$^{-1}$ and a measured Curie temperature of about 45 K;[19] the $MnPS_3$ monolayer has E_m = −13 meV f.u.$^{-1}$ and a measured Néel temperature of about 103 K.[68] The present 1D MPS_4 nanowires have exchange energies competitive with the values of synthetic 2D magnetic materials, offering stable building blocks for integration of heterostructures and devices with desirable functions.

Conclusions

In summary, based on the superatom concept, we exploited the tetrahedral [PS_4] cluster as a building block to construct assemblies of different dimensions by DFT calculations. Ternary MPS_4 nanowires with outstanding dynamic and thermal stabilities are obtained by linking [PS_4] units with group-IIIA (B, Al, Ga, and In) atoms or transition metal (V, Cr, Co, Ni, Mo, Ru, Pd, and Re) atoms. The assembled nanowires with unique structure symmetries exhibit diverse and peculiar electronic band structures, such as the coexistence of a SOC Dirac point and a nearly flat band, and being bipolar magnetic semiconductors. Moreover, these MPS_4 nanowires can be further assembled into quasi-1D bulk structures *via* vdW interactions as well as layered 2D structures by covalent bonding that are feasible in the experiment.

Conflicts of interest

There are no conflicts to declare.

Acknowledgements

This work was financially supported by the National Natural Science Foundation of China (91961204, 11974068, 12222403) and XinLiaoYingCai Project of Liaoning province, China (XLYC1905014). The authors acknowledge the computer resources provided by the Shanghai Supercomputer Center and the Supercomputing Center of Dalian University of Technology.

References

1 A. K. Geim and I. V. Grigorieva, *Nature*, 2013, **499**, 419–425.
2 C. A. Slade, A. M. Sanchez and J. Sloan, *Nano Lett.*, 2019, **19**, 2979–2984.
3 M. Nagata, S. Shukla, Y. Nakanishi, Z. Liu, Y. C. Lin, T. Shiga, Y. Nakamura, T. Koyama, H. Kishida, T. Inoue, N. Kanda, S. Ohno, Y. Sakagawa, K. Suenaga and H. Shinohara, *Nano Lett.*, 2019, **19**, 4845–4851.
4 J. Lin, O. Cretu, W. Zhou, K. Suenaga, D. Prasai, K. I. Bolotin, N. T. Cuong, M. Otani, S. Okada, A. R. Lupini, J. C. Idrobo, D. Caudel, A. Burger, N. J. Ghimire, J. Yan, D. G. Mandrus, S. J. Pennycook and S. T. Pantelides, *Nat. Nanotechnol.*, 2014, **9**, 436–442.
5 N. Kanda, Y. Nakanishi, D. Liu, Z. Liu, T. Inoue, Y. Miyata, D. Tomanek and H. Shinohara, *Nanoscale*, 2020, **12**, 17185–17190.
6 X. Liu, T. Xu, X. Wu, Z. Zhang, J. Yu, H. Qiu, J. H. Hong, C. H. Jin, J. X. Li, X. R. Wang, L. T. Sun and W. Guo, *Nat. Commun.*, 2013, **4**, 1776.
7 S. Meyer, T. Pham, S. Oh, P. Ercius, C. Kisielowski, M. L. Cohen and A. Zettl, *Phys. Rev. B*, 2019, **100**, 041403 (R).
8 S. Stonemeyer, J. D. Cain, S. Oh, A. Azizi, M. Elasha, M. Thiel, C. Song, P. Ercius, M. L. Cohen and A. Zettl, *J. Am. Chem. Soc.*, 2021, **143**, 4563–4568.
9 M. V. Kharlamova, L. V. Yashina, A. A. Eliseev, A. A. Volykhov, V. S. Neudachina, M. M. Brzhezinskaya, T. S. Zyubina, A. V. Lukashin and Y. D. Tretyakov, *Phys. Status Solidi B*, 2012, **249**, 2328–2332.
10 S. Oh, S. Chae, B. J. Kim, K. H. Choi, W.-S. Jang, J. Jang, Y. Hussain, D. K. Lee, Y.-M. Kim, H. K. Yu and J.-Y. Choi, *RSC Adv.*, 2018, **8**, 33980–33984.
11 Y. Zhou, L. Wang, S. Chen, S. Qin, X. Liu, J. Chen, D.-J. Xue, M. Luo, Y. Cao, Y. Cheng, E. H. Sargent and J. Tang, *Nat. Photonics*, 2015, **9**, 409–415.
12 J. Lee, B. J. Kim, Y. K. Chung, W. G. Lee, I. J. Choi, S. Chae, S. Oh, J. M. Kim, J. Y. Choi and J. Huh, *J. Raman Spectrosc.*, 2020, **51**, 1100–1107.
13 M. N. Kozlova, Y. V. Mironov, E. D. Grayfer, A. I. Smolentsev, V. I. Zaikovskii, N. A. Nebogatikova, T. Y. Podlipskaya and V. E. Fedorov, *Chemistry*, 2015, **21**, 4639–4645.
14 C. Shang, L. Fu, S. Zhou and J. Zhao, *JACS Au*, 2021, **1**, 147–155.
15 M.-S. Qiu, H.-H. Guo, Y. Zhang, B.-J. Dong, S. Ali and T. Yang, *Chin. Phys. B*, 2019, **28**, 106103.
16 G. H. Han, D. L. Duong, D. H. Keum, S. J. Yun and Y. H. Lee, *Chem. Rev.*, 2018, **118**, 6297–6336.
17 Y.-P. Wang and M.-Q. Long, *Phys. Rev. B*, 2020, **101**, 024411.

18 G.-D. Zhao, X. Liu, T. Hu, F. Jia, Y. Cui, W. Wu, M.-H. Whangbo and W. Ren, *Phys. Rev. B*, 2021, **103**, 014438.
19 B. Huang, G. Clark, E. Navarro-Moratalla, D. R. Klein, R. Cheng, K. L. Seyler, D. Zhong, E. Schmidgall, M. A. McGuire, D. H. Cobden, W. Yao, D. Xiao, P. Jarillo-Herrero and X. Xu, *Nature*, 2017, **546**, 270–273.
20 Y. Zhu, H. Li, T. Chen, D. Liu and Q. Zhou, *Vacuum*, 2020, **182**, 109694.
21 M. Zhu, H. Kou, K. Wang, H. Wu, D. Ding, G. Zhou and S. Ding, *Mater. Horiz.*, 2020, **7**, 3131–3160.
22 K. Z. Du, X. Z. Wang, Y. Liu, P. Hu, M. I. Utama, C. K. Gan, Q. Xiong and C. Kloc, *ACS Nano*, 2016, **10**, 1738–1743.
23 R. Gusmão, Z. Sofer, D. Sedmidubský, Š. Huber and M. Pumera, *ACS Catal.*, 2017, **7**, 8159–8170.
24 T. Olsen, *J. Phys. D: Appl. Phys.*, 2021, **54**, 314001.
25 S. Huang, Z. Shuai and D. Wang, *J. Mater. Chem. A*, 2021, **9**, 2734–2741.
26 F. Caruso, M. R. Filip and F. Giustino, *Phys. Rev. B: Condens. Matter Mater. Phys.*, 2015, **92**, 125134.
27 W.-G. Lee, S. Chae, Y. K. Chung, S. Oh, J.-Y. Choi and J. Huh, *Phys. Status Solidi RRL*, 2019, **13**, 18500517.
28 M. S. Stark, K. L. Kuntz, S. J. Martens and S. C. Warren, *Adv. Mater.*, 2019, **31**, 1808213.
29 G. Kresse and J. Furthmuller, *Phys. Rev. B: Condens. Matter Mater. Phys.*, 1996, **54**, 11169–11186.
30 G. Kresse and J. Hafner, *Phys. Rev. B: Condens. Matter Mater. Phys.*, 1993, **47**, 558–561.
31 G. Kresse and D. Joubert, *Phys. Rev. B: Condens. Matter Mater. Phys.*, 1999, **59**, 1758–1775.
32 P. E. Blochl, *Phys. Rev. B: Condens. Matter Mater. Phys.*, 1994, **50**, 17953–17979.
33 J. P. Perdew, K. Burke and M. Ernzerhof, *Phys. Rev. Lett.*, 1996, **77**, 3865–3868.
34 J. P. Perdew, M. Ernzerhof and K. Burke, *J. Chem. Phys.*, 1996, **105**, 9982–9985.
35 H. J. Monkhorst and J. D. Pack, *Phys. Rev. B: Condens. Matter Mater. Phys.*, 1976, **13**, 5188–5192.
36 A. V. Krukau, O. A. Vydrov, A. F. Izmaylov and G. E. Scuseria, *J. Chem. Phys.*, 2006, **125**, 224106.
37 V. I. Anisimov, J. Zaanen and O. K. Andersen, *Phys. Rev. B: Condens. Matter Mater. Phys.*, 1991, **44**, 943–954.
38 K. Parlinski, Z. Q. Li and Y. Kawazoe, *Phys. Rev. Lett.*, 1997, **78**, 4063–4066.
39 M. J. Frisch, G. W. Trucks, H. B. Schlegel, G. E. Scuseria, M. A. Robb, J. R. Cheeseman, G. Scalmani, V. Barone, G. A. Petersson, H. Nakatsuji, X. Li, M. Caricato, A. V. Marenich, J. Bloino, B. G. Janesko, R. Gomperts, B. Mennucci, H. P. Hratchian, J. V. Ortiz, A. F. Izmaylov, J. L. Sonnenberg, D. Williams-Young, F. Ding, F. Lipparini, F. Egidi, J. Goings, B. Peng, A. Petrone, T. Henderson, D. Ranasinghe, V. G. Zakrzewski, J. Gao, N. Rega, G. Zheng, W. Liang, M. Hada, M. Ehara, K. Toyota, R. Fukuda, J. Hasegawa, M. Ishida, T. Nakajima, Y. Honda, O. Kitao, H. Nakai, T. Vreven, K. Throssell, J. A. Montgomery, Jr., J. E. Peralta, F. Ogliaro, M. J. Bearpark, J. J. Heyd, E. N. Brothers, K. N. Kudin, V. N. Staroverov, T. A. Keith, R. Kobayashi, J. Normand, K. Raghavachari, A. P. Rendell, J. C. Burant, S. S. Iyengar, J. Tomasi, M. Cossi, J. M. Millam, M. Klene, C. Adamo, R. Cammi, J. W. Ochterski, R. L. Martin, K. Morokuma, O. Farkas, J. B. Foresman and D. J. Fox, Wallingford CT, 2016.
40 W. A. de Heer, *Rev. Mod. Phys.*, 1993, **65**, 611–676.
41 T. Tsukamoto, N. Haruta, T. Kambe, A. Kuzume and K. Yamamoto, *Nat. Commun.*, 2019, **10**, 3727.
42 S. Xing, L. Wu, Z. Wang, X. Chen, H. Liu, S. Han, L. Lei, L. Zhou, Q. Zheng, L. Huang, X. Lin, S. Chen, L. Xie, X. Chen, H.-J. Gao, Z. Cheng, J. Guo, S. Wang and W. Ji, 2022, DOI: **10.48550/arXiv.2110.09058**.
43 J. Sloan, S. J. Grosvenor, S. Friedrichs, A. I. Kirkland, J. L. Hutchison and M. L. H. Green, *Angew. Chem., Int. Ed.*, 2002, **41**, 1156–1159.
44 T. Pham, S. Oh, P. Stetz, S. Onishi, C. Kisielowski, M. L. Cohen and A. Zettl, *Science*, 2018, **361**, 263–266.
45 X. Li and J. Yang, *Phys. Chem. Chem. Phys.*, 2013, **15**, 15793–15801.
46 X. Li and J. Yang, *Natl. Sci. Rev.*, 2016, **3**, 365–381.
47 S. M. Young and C. L. Kane, *Phys. Rev. Lett.*, 2015, **115**, 126803.
48 S. Borisenko, Q. Gibson, D. Evtushinsky, V. Zabolotnyy, B. Büchner and R. J. Cava, *Phys. Rev. Lett.*, 2014, **113**, 027603.
49 Z. Gao, Q. Wang, W. Wu, Z. Tian, Y. Liu, F. Ma, Y. Jiao and S. A. Yang, *Phys. Rev. B*, 2021, **104**, 245423.
50 H. Fashandi, V. Ivády, P. Eklund, A. L. Spetz, M. I. Katsnelson and I. A. Abrikosov, *Phys. Rev. B: Condens. Matter Mater. Phys.*, 2015, **92**, 155142.
51 L. Chen, L. Q. Zhou, Y. Zhou, C. Liu, Z. N. Guo, S. Y. Gao, W. H. Fan, J. F. Xu, Y. X. Guo, K. Liao, J. O. Wang, H. M. Weng and G. Wang, 2022, DOI: DOI: **10.48550/arXiv.2201.05833**.
52 M. Kang, L. Ye, S. Fang, J.-S. You, A. Levitan, M. Han, J. I. Facio, C. Jozwiak, A. Bostwick, E. Rotenberg, M. K. Chan, R. D. McDonald, D. Graf, K. Kaznatcheev, E. Vescovo, D. C. Bell, E. Kaxiras, J. van den Brink, M. Richter, M. P. Ghimire, J. G. Checkelsky and R. Comin, *Nat. Mater.*, 2020, **19**, 163–169.
53 L. Ye, M. Kang, J. Liu, F. von Cube, C. R. Wicker, T. Suzuki, C. Jozwiak, A. Bostwick, E. Rotenberg, D. C. Bell, L. Fu, R. Comin and J. G. Checkelsky, *Nature*, 2018, **555**, 638–642.
54 D. Marchenko, D. V. Evtushinsky, E. Golias, A. Varykhalov, T. Seyller and O. Rader, *Sci. Adv.*, 2018, **4**, eaau0059.
55 M. I. B. Utama, R. J. Koch, K. Lee, N. Leconte, H. Li, S. Zhao, L. Jiang, J. Zhu, K. Watanabe, T. Taniguchi, P. D. Ashby, A. Weber-Bargioni, A. Zettl, C. Jozwiak, J. Jung, E. Rotenberg, A. Bostwick and F. Wang, *Nat. Phys.*, 2021, **17**, 184–188.
56 J.-W. Rhim and B.-J. Yang, *Adv. Phys.: X*, 2021, **6**, 1901606.
57 A. Kuhn, R. Eger, P. Ganter, V. Duppel, J. Nuss and B. V. Lotsch, *Z. Anorg. Allg. Chem.*, 2014, **640**, 2663–2668.

58 F. Pielnhofer, L. M. Schoop, A. Kuhn, R. Eger, J. Nuss, H. Nuss and B. V. Lotsch, *Z. Anorg. Allg. Chem.*, 2019, **645**, 267–271.
59 B.-Z. Sun, Z. Ma, C. He and K. Wu, *Phys. Chem. Chem. Phys.*, 2015, **17**, 29844–29853.
60 L. Li, W. Han, L. Pi, P. Niu, J. Han, C. Wang, B. Su, H. Li, J. Xiong, Y. Bando and T. Zhai, *InfoMat*, 2019, **1**, 54–73.
61 J. Son, S. Son, P. Park, M. Kim, Z. Tao, J. Oh, T. Lee, S. Lee, J. Kim, K. Zhang, K. Cho, T. Kamiyama, J. H. Lee, K. F. Mak, J. Shan, M. Kim, J. G. Park and J. Lee, *ACS Nano*, 2021, **15**, 16904–16912.
62 A. K. Budniak, N. A. Killilea, S. J. Zelewski, M. Sytnyk, Y. Kauffmann, Y. Amouyal, R. Kudrawiec, W. Heiss and E. Lifshitz, *Small*, 2020, **16**, 1905924.
63 Q. Chen, Q. Ding, Y. Wang, Y. Xu and J. Wang, *J. Phys. Chem. C*, 2020, **124**, 12075–12080.
64 J. Xu, C. Xu, J.-B. Liu, L. Bellaiche, H. Xiang, B.-X. Liu and B. Huang, *npj Comput. Mater.*, 2019, **5**, 114.
65 P. W. Anderson, *Phys. Rev.*, 1959, **115**, 2–13.
66 J. B. Goodenough, *Phys. Rev.*, 1955, **100**, 564–573.
67 J. Kanamori, *J. Phys. Chem. Solids*, 1959, **10**, 87–98.
68 J. Yang, Y. Zhou, Q. Guo, Y. Dedkov and E. Voloshina, *RSC Adv.*, 2020, **10**, 851–864.